Eur. Phys. J. B **10**, 61–70 (1999)

THE EUROPEAN PHYSICAL JOURNAL B

EDP Sciences

Rheology of nanosized hairy grain suspensions

J.-C. Castaing[1], C. Allain[2], P. Auroy[3,a], and L. Auvray[4]

[1] Rhône-Poulenc Recherche, 52 rue de la Haie-Coq, 93308 Aubervilliers Cedex, France
[2] FAST[b], Université Paris-Sud, 91405 Orsay Cedex, France
[3] Institut Curie[c], Section de Recherche, 11 rue Pierre et Marie Curie, 75231 Paris Cedex 05, France
[4] Laboratoire Léon Brillouin, CNRS-CEA, Centre d'Études Nucléaires de Saclay, 91191 Gif-sur-Yvette Cedex, France

Received 23 March 1998

Abstract. Suspensions of nanosized hairy grains have been prepared by grafting long polydimethylsiloxane chains (molecular weight $\cong$ 160 000) onto silica particles (radius $\cong$ 15 nm), dispersed into a good solvent of PDMS. Depending on the particle volume fraction, different rheological behaviors are observed. In the very dilute regime, the suspensions are perfectly stable and the particles behave almost as hard spheres: flow penetration inside the corona is then very weak. When the particle volume fraction goes to the close packing volume fraction, the suspension viscosity does not diverge as for hard spheres due to the increase of flow penetration inside the corona and to corona entanglements. The particles have then the same behavior as polymer stars having an intermediate number of arms ($\cong$ 55). Finally, in the concentrated regime ($c \geq 0.1$ g/cm^3), the suspensions form irreversible gels. We shown that this unexpected gelation phenomenon is related to the presence of the silica cores: grafted PDMS chains can adsorb onto different particles and form irreversible bonds between the cores. The viscosity and elastic modulus evolutions during gelation are well described by the scalar percolation model of sol-gel transition.

PACS. 82.70.Dd Colloids – 61.41.+e Polymers, elastomers, and plastics – 81.05.Qk Reinforced polymers and polymer-based composites

1 Introduction

The properties of curved polymer brushes and star-shaped polymers have been the subject of intensive study during the past decades due to their importance in a large number of applications such as colloidal stabilization [1], elastomer reinforcement [2], and in many biological systems. Several model systems having different molecular architecture have been investigated, as for instance regular polymer stars or micelles of diblock copolymers [3–10]. Studies of their structure and rheology in solution have demonstrated the importance of the curvature radius (the monomer density distribution decreases from the core to the periphery [11]), of the arm number, and of the flow penetration inside the polymer corona. In this paper, we report on the rheological properties of a novel system made of hairy nanoparticles in suspension. Well-defined colloidal particles having a small silica core with long polymer chains (PDMS) end-grafted onto were synthesized [2,12]. The silica core is 15 nm in radius, and the molecular weight of the grafted polymer is 160 000; the grafting density is large enough to induce a stretching of the chains in good solvent. The ratio of polymer corona thickness to silica core radius is then about 2.3.

These hairy nanoparticles have an outer structure close to that of star polymers or copolymer micelles. According to the scaling model of Daoud-Cotton [11], the monomer concentration profile far from the center does not depend on the nature of the core, but only on the arm number. Thus, the rheological behavior of different star-like colloids is expected to be similar, at least in the very dilute regime. On the contrary, for concentrated suspensions, the core nature could have some influence. In fact, we observed a behavior unexpected for sterically stabilized particles: above a concentration of about 0.12 g/cm^3, the suspensions gel irreversibly. These gel phases which have a large elastic modulus, do not disperse in the presence of an excess of solvent. Thus, these gels differ from the colloidal crystals formed by star polymers at high concentration which are reversible under dilution. We show that it is related to the structure of our particles and to the surface chemistry of the silica core.

In the following, hairy particles are compared to two reference systems: hard spheres that are obtained by grafting octadecyl chains onto the same silica cores as for the hairy grains, and free PDMS chains with the same molecular weight as the grafted ones. The rheological properties

[a] e-mail: auroy@curie.fr
[b] UMR 7608 du CNRS
[c] UMR 168 du CNRS

Table 1. Results of the hairy particle characterization.

Arm molecular weight (GPC)	Core radius (TEM)	Core weight	Grafted polymer per unit area (IR)	Corona weight	Number of arms	Hairy particle radius (SANS)
160 000 g/mole	15 ± 2 nm	2.5×10^{-17} g	5.3 ± 0.5 mg/m^2	1.5×10^{-17} g	55	50 ± 5 nm

of the three systems were systematically investigated and compared. The paper is organized as follows: in Section 1, we present the structure and the characterization of the hairy particles, and the methods of rheological measurement. Section 2 is devoted to the very dilute regime: the hydrodynamic radius of the hairy particles is found equal to the exterior radius measured by small angle neutron scattering, showing that, in this regime, flow penetration inside the polymer corona is negligible *i.e.* the hairy particles behave as hard spheres. In Section 3, we compare the increase of the viscosity with volume fraction for the three systems under study. We observe that the viscosity of hairy grain suspensions does not diverge when the volume fraction goes to the close packing volume fraction. On the contrary, the results show that flow penetration inside the corona takes place well before the close packing fraction and that, for larger volume fraction, polymer coronas interpenetrate. Such behavior is similar to that of star-shaped polymers having an intermediate number of arms. Finally, Section 4 is devoted to volume fractions much larger than the overlap concentration. The presence of the silica core is then important and an unexpected gelation phenomenon takes place. We study the time evolution of the rheological properties at given volume fractions (viscosity and elastic modulus *versus* time). The interpretation in terms of sol-gel transition critical behavior leads to results similar to that observed for irreversible polymer gels.

2 Experimental

2.1 Synthesis of the grafted grains

The grafted particles were prepared from small sized silica particles and long Si-OH terminated PDMS. The condensation of a polymer Si-OH end with a silica surface silanol leads to the formation of a covalent bond. A specific grafting procedure was designed to avoid particle aggregation during all the stages of the synthesis [12].

The polymer used was a commercially available α-ω hydroxylated PDMS with a molecular weight $M_w \cong 160\,000$ (GPC) and a polydispersity index of the order of 2 (see Tab. 1). We also prepared by anionic polymerization a monofunctional PDMS ($M_w = 167\,000$, polydispersity index = 1.07): it carries at one end an -OH group and at the other end a non reactive sec-butyl group. The silica particles were synthesized according to the Stöber's method [13] which allows one to prepare monodisperse suspensions in ethanol. The amount of water in the reaction bath was adjusted to obtain particles having 15 nm in radius. The suspension was then transferred in diethylketone by distillation; this ketone was chosen because it is a good solvent of PDMS and it is enough polar for electrostatic stabilization of the bare silica particles. The quantity of PDMS added in the reaction bath was chosen not too large ($c \cong 0.1$ g/cm^3) in order to avoid flocculation induced by depletion of the ungrafted particles. The silica concentration was typically of the order of 0.01 g/cm^3. Under these conditions, the PDMS chains are eventually attached by only one end and no chemical crosslinking occurs. This is proved by the use of the monofunctional PDMS, which gives exactly the same results as the difunctional one. The PDMS and the silica particles in diethylketone were left 12 hours at 100 °C in the presence of diisopropylethylamine used as a catalyst. Finally, the PDMS in excess was removed by dialysis.

2.2 Characterization of the silica core

The silica particles were observed by Transmission Electron Microscopy (TEM). The particles are not perfectly spherical, but their shape irregularities are slight and we can unambiguously determine their size and assume in the following that they are spherical. The average radius was found equal to 15 nm with a narrow distribution: the ratio of standard deviation to average size is about 0.13 (see Tab. 1).

The density of the silica particles, ρ, is an important parameter for the suspension characterization. Two different methods were used to measure ρ: first densimetry, and second small angle neutron scattering. To determine ρ by densimetry, we measured the density of suspensions for different concentrations in pure water using a PAAR densimeter. From the experimental data, we can obtain a precise value of the silica particle density provided the silica mass fraction in the suspensions, s, is known. The mass fraction was determined by drying and weighing. However, since Stöber's silica particles are porous [14], the measured mass fraction depends on whether water is extracted from the pores or not during drying. This leads us to define two densities: the density of the hydrated silica grains (which corresponds to their state in aqueous suspension) and the density of the silica that forms the particle skeleton. We find:

i) $\rho_{\text{hydrated}} = 1.93 \pm 0.02$ g/cm^3 (drying conditions $T =$ 25 °C, relative humidity RH $\cong 50\%$);

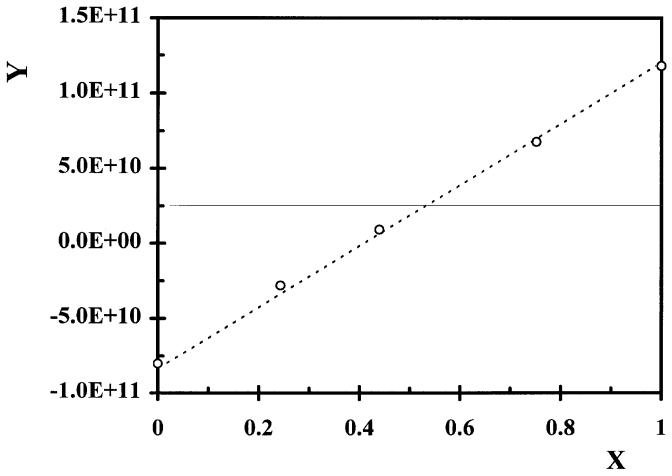

Fig. 1. Determination of the silica core particle density by SANS: plot of $Y = 6(I_0/sa^3)^{1/2}$ *versus* X (relative proportion of H_2O in the D_2O/H_2O mixture used as solvent).

ii) $\rho_{\text{skeleton}} = 2.18 \pm 0.02$ g/cm^3 (drying conditions $T = 100\,^\circ$C, $P = 5 \times 10^{-9}$ bars).

As expected, this last value is in good agreement with the density of amorphous silica ($\rho = 2.2$ g/cm^3) [15].

We also determined the *in situ* density of the particles using small angle neutron scattering. The variation of the intensity scattered by a sphere, $I(q)$, with the momentum transfer q, depends on the square of the difference between the scattering length density (SLD) of the solvent and that of the particle. At small q, this last value is an average between the SLD of the solvent filling the pores, n_{sol}, and that of the silica skeleton, n_{sil}. Due to the presence of solvent in the pores, the contrast (and therefore the scattered intensity) varies less than in the case of bulk silica particles. However, the contrast falls to zero whatever the porosity is when the SLD of the solvent becomes equal to that of the silica skeleton ($n_{\text{sol}} - n_{\text{sil}} = 0$). The scattered intensity determined by fitting the curve $I(q)$ *versus* q, is directly related to the volume fraction of the pores inside the particles, φ, and to the solvent composition:

$$\sqrt{\frac{I_0}{sa^3}} = \sqrt{\frac{\pi}{3\rho_{\text{hyd}}}}\,(1-\varphi)\,(n_{\text{D}} - n_{\text{H}})\left[X - \frac{n_{\text{D}} - n_{\text{sil}}}{n_{\text{D}} - n_{\text{H}}}\right] \quad (1)$$

where I_0 is the scattering intensity extrapolated at $q \to 0$ for a given X, s is the mass fraction of the suspension determined by using the first drying procedure (hydrated silica) and a is the radius of a silica particle. n_{H} and n_{D} are respectively the SLD of H_2O and D_2O and X the relative proportion of H_2O in the mixture of H_2O/D_2O used as solvent.

Figure 1 displays the variation of $Y = 6(I_0/sa^3)^{1/2}$ *versus* X. By fitting the experimental points, we can determine the skeleton silica SLD and the pore volume fraction. We find: $n_{\text{sil}} = 3.63 \times 10^{10}$ cm^{-2} which leads to $\rho_{\text{skeleton}} = 2.3$ g/cm^3, in good agreement with the density of amorphous silica. The pore volume fraction is found equal to $\varphi = 0.385$. These values allow us to calculate the density of the particles when hydrated: $\rho_{\text{hydrated}} = 1.8$ g/cm^3. Compared to the results of densimetry measurements, we find that ρ_{hydrated} found by neutron scattering is slightly smaller. This can be attributed to changes in water specific volume that have not been taken into account in our analysis. In the following, we take $\rho = 1.8$ g/cm^3 to relate the mass fraction of the silica particles to their volume fraction.

In order to compare the rheology of hairy particle suspensions to that of hard spheres, we stabilized the bare silica spheres by grafting short octadecyl chains. The synthesis was done following a well-known procedure [16]. In non polar solvent (the solvent used for all the rheological measurements is dodecane), they are expected to behave as hard spheres [17–19].

2.3 Structure of the hairy particles

The amount of grafted PDMS was determined by infrared absorption spectroscopy (IR) after calibration with polymer solutions. In that aim, the suspensions were dialyzed in carbon tetrachloride and the intense absorption peak of PDMS at 1 262 cm^{-1} recorded. The signal arising from the polymer can be very well distinguished from that of the silica allowing accurate measurements. For the particles investigated here, the grafting density is equal to 5.3 mg/m^2. Taking account of the molecular weight of the PDMS chain and of the silica core radius, the average number of polymer arms per particle is found equal to 55 – assuming a density of 1.8 g/cm^3 for the core (see Tab. 1).

Small angle neutron scattering is an alternative way to measure the quantity of grafted polymer. It is also a powerful technique to study the structure of the hairy balls. Indeed, changing the scattering length density of the solvent (a mixture of H and D chloroform) allows us to match either the silica core (polymer contrast) or the polymer corona (silica contrast). So, the structure of each component of a hairy ball can be studied separately. Using silica contrast, we first measured the radius of the particle core. The value found is in good agreement with the TEM determination performed before grafting. Furthermore, the analysis of the intensity scattered at small angle shows that no aggregation of silica cores had occurred during grafting. In polymer contrast, the intensity comes only from the corona. Two simple models were used to describe the monomer concentration profile: a step profile and a triangle function. A good fit is obtained with the triangle model, showing a slow decrease of the monomer concentration across the polymer layer [2]. From the intensity scattered in the Guinier regime, we can estimate the overall quantity of grafted polymer and, using the triangle model, the extension of the polymer corona. The grafting density is found the same as by IR determination (within the relative accuracy of about 20 %). The outer radius of the grafted particle is found equal to 50 ± 5 nm (see Tab. 1).

2.4 Viscosity measurements

The viscosity of dilute suspensions was measured using a Couette viscosimeter (Low Shear 30 Contraves). All the experiments were performed at 20.0 ± 0.3 °C. The imposed shear rate ranged between 10^{-2} and 5×10^2 s^{-1}. All the suspensions were found to be Newtonian, except for the most concentrated ones ($c \geq 0.04$ g/cm^3); a small shear thinning was then observed for shear rates larger than 1 s^{-1}. All the viscosity data given below correspond to the Newtonian limit measured at small shear rates.

Measurements of the viscosity and of the elastic modulus during the sol-gel transition were performed using a magnetic levitation sphere rheometer [20,21]. A small magnetic sphere is located into a cylinder cell of much larger diameter which contains the sample. The sphere is maintained motionless by a magnetic field that counterbalances the other forces acting on the sphere. When the cell is moved, the intensity in the coil that creates the magnetic field changes due to viscous drag force when the sample is viscous, or to elastic restoring force when the sample is elastic. In the first case, the intensity is simply proportional to the displacement velocity, while, in the second, it is proportional to the displacement. So, after calibration, this set-up allows us to follow the time evolution of the viscosity and of the modulus during the sol-gel transition. Different sample speeds can be used (the lowest gradient is 10^{-4} s^{-1}). In practice, we always used the lowest speed giving a signal large enough to be reliably measured.

Because of the divergence of the viscoelastic relaxation time near the gelation point, it is not possible to wait between two measurements until the signal does not change anymore: indeed, during that time, the sample still evolves. This makes the accurate determination of gelation point difficult. So, we used the following protocol (see Fig. 2a): we changed the displacement state (starting or stopping) every 30 min and, to avoid too strong perturbations of the sample, we displaced the tube several times in a same direction (about 10 times), then we changed the direction and followed the same time sequence, and so on. During a set of displacements in a same direction, the force acting on the magnetic sphere at the end of the rest period increases since the force due to the previous displacement is not completely relaxed (Fig. 2a). This impedes us to directly determine whether the sample is viscous (*i.e.* is a sol) or whether it has a steady-state elastic modulus (*i.e.* is a gel). To overcome this difficulty, we assumed that the force relaxation at long time is exponential. Then, the signal (F) follows: $[\mathrm{d}F/\mathrm{d}t]_{t=t_1} = -(F_\infty - F(t_1))/\tau$ where $F(t_1)$ is the signal value for $t = t_1$ and τ the characteristic relaxation time. Before gelation point, F_∞ is simply the signal when all the relaxations have taken place (F_0) and is the same for all the measurements. After gelation point, F_∞ includes also the steady state elastic contribution and thus differs for F_0. So, to determine the gelation point, we drew $[\mathrm{d}F/\mathrm{d}t]_{t=t_1}$ *versus* $F(t_1)$ for a fixed value of t_1 (Fig. 2b). The first series for which the plot is not a straight line (with $F_\infty = F_0$) marks the gelation of the sample. This allows us to determine t_g; in the case of Figure 2b, $t_\mathrm{g} = 3\,800 \pm 200$ min. It is to note that the values of $[\mathrm{d}F/\mathrm{d}t]_{t=t_1}$ reported in Figure 2b were calculated for a rest time equal to $t_1 = 20$ min. Changing the value of t_1 does not change significantly t_g: it remains within the error bar.

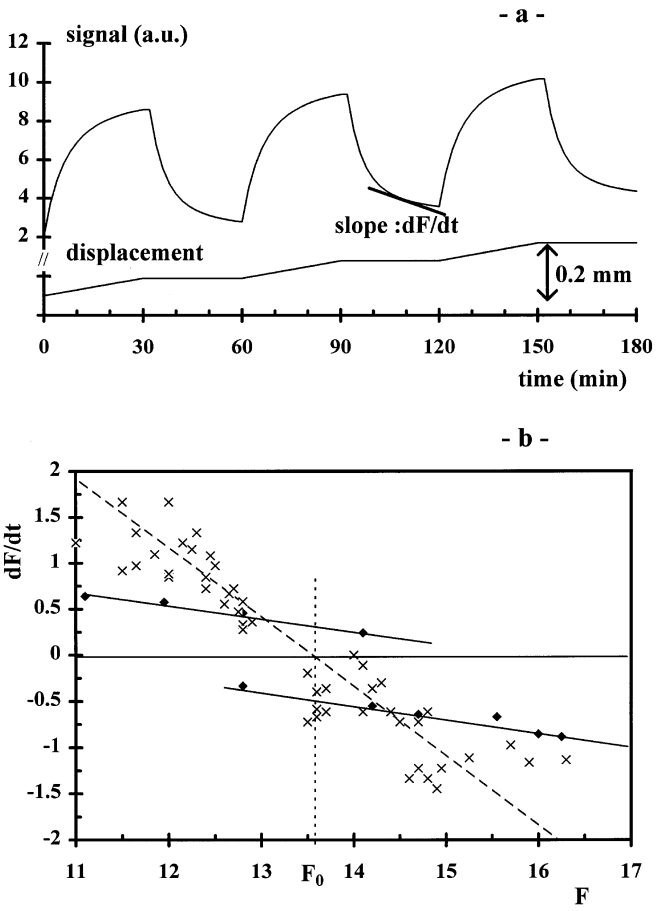

Fig. 2. Determination of gelation time: (a) schematic representation of the imposed displacement and of the signal (proportional to the force acting on the sphere) *versus* time; (b) relaxation slope measured for $t_1 = 20$ min: (×) last series before gelation; (♦) first serie after gelation.

2.5 Sample preparation

All the samples were prepared from dilute preparation batches (0.03 g/cm^3 in hexane) transferred in dodecane by hexane evaporation. Great care was taken to avoid drying and occurence of locally high concentration. Indeed, as explained in Section 4, at high concentration, hairy particles form gels that do not dissolve in an excess of solvent. To overcome this difficulty, the hairy particles are always kept in very dilute solution; concentrated suspensions are prepared just before use by introducing the required amount of dodecane and distillating off hexane. This procedure is the sole one which allows us to avoid locally high concentrations and to prepare perfectly homogeneous samples. Dodecane was chosen since it is a good solvent of PDMS

and its saturation vapor pressure is low; so, no significant evaporation occurs during experiments even when they take several months as in the case of the sol-gel transition investigations.

3 Very dilute regime

The viscosity of very dilute suspensions have been measured in order to investigate the properties of the intrinsic viscosity. We compared the hairy particle suspension with the two reference samples: a suspension of hard sphere silica particles (prepared with the same cores as the hairy particles) and a solution of free PDMS chains (the same as that grafted on the hairy particles). A linear regression of the viscosity *versus* concentration, $\eta(c)$, in the dilute limit allows us to determine the intrinsic viscosity: $[\eta] = \lim_{c\to 0}(\eta - \eta_0)/\eta_0 c$ where η_0 is the solvent viscosity. Comparison with the Einstein's formula for suspensions of spheres ($\eta = \eta_0(1 + 2.5\Phi)$ where Φ is the volume fraction of the particles) leads to the relation:

$$[\eta] = 2.5 v_c/m_c \qquad (2)$$

where m_c and v_c are respectively the mass and the hydrodynamic volume of one colloid. v_c can be viewed as the volume of the hard sphere (of mass m_c) which would give the same intrinsic viscosity $[\eta]$. So, from $[\eta]$, we can deduce the average density and the hydrodynamic radius R_h since m_c is known. The obtained values are reported in Table 2.

For the hard sphere suspension, the average silica density is found very low (1.3 g/cm^3) compared to the values measured by the other techniques (1.8 g/cm^3, see Sect. 1). Such low values of the silica density deduced from intrinsic viscosity measurements have yet been reported [17,19]. The origin of this discrepancy is still unclear.

Since the mass and the volume of the silica core are known, it is also possible to estimate the average concentration of the polymer inside the grafted corona. Taking silica density equal to 1.3 or 1.8 g/cm^3 in this calculation does not make a big difference since the core volume is small. (The corona inner radius would change from 17 nm to 15 nm. This uncertainty corresponds to the standard deviation of the TEM measurements and is small compared to the overall dimension of the corona.) The average polymer concentration in the grafted layer is found equal to 0.032 g/cm^3. This value is smaller than the average value inside a free polymer chain deduced from the intrinsic viscosity: 0.068 g/cm^3. An inverse order would be expected. Indeed, the corona thickness being larger than a free polymer coil, the arms in the corona are stretched. So, a larger concentration is needed to produce an osmotic pressure large enough to counterbalance the elastic force created by the stretching.

This disagreement comes from the difference in the structure that leads to different permeabilities. For a free chain, the hydrodynamic volume is small since the solvent flow partially penetrates inside the coil. For a grafted layer, the flow penetration is smaller. The difference between the hydrodynamic radius and the static radius is larger for free polymer chains than for hairy particles. Thus, the concentration inside a free chain deduced from intrinsic viscosity is overestimated. That explains why its value is larger than the concentration found for the polymer inside the corona. A similar behavior has already been observed in the case of star polymers [3,5].

Finally, it is interesting to compare the radius of the hairy particles deduced from intrinsic viscosity measurements with the radius found by small angle neutron scattering (see Tabs. 1 and 2). This comparison might be questioned because we did not use the same solvent for the two experiments (for technical reasons). However, chloroform and dodecane (used respectively for SANS and viscosimetry) are of comparable quality for PDMS – chloroform being a little bit better than dodecane; moreover it has been shown (both theoretically and experimentally) that the extension of a polymer brush varies weakly with the solvent quality (in the good solvent regime) [22]. Thus, the comparison between the static and the hydrodynamical radii is meaningful. We remind the reader that the static radius has been worked out from the Guinier domain of the SANS spectrum. This static radius is the maximal extension of the corona. It appears that this extension and the hydrodynamic radius (deduced from the intrinsic viscosity) are very close; therefore, we can consider that in the dilute regime, hairy grains behave as hard spheres since the hydrodynamical flow do not penetrate inside the polymer corona. However, at larger concentration, this is no longer true as shown below.

Table 2. Hydrodynamic properties of the three systems investigated (in the dilute limit).

	Hairy particles	Hard spheres	PDMS chain
$[\eta]$	30 ± 2 cm^3/g	1.9 ± 0.2 cm^3/g	37 ± 2 cm^3/g
average density	0.083 g/cm^3	1.3 g/cm^3	0.068 g/cm^3
R_h	49 nm	17 nm	9.8 nm

4 Dilute regime

Figure 3 displays the variation of the viscosity as a function of the volume fraction for the three systems investigated: hairy particles, hard spheres, and free PDMS chains. The volume fraction, Φ, is calculated from the intrinsic viscosity determined in Section 2: Φ equals $c[\eta]/2.5$. The observed variations are different: the viscosity for hard sphere suspensions diverges for a value of Φ smaller than 1 while, for hairy particles (and for free PDMS chains), the viscosity remains finite even when Φ exceeds 1. This has to be related to the softness of the hairy particle corona. Nevertheless, the viscosity increases with the volume fraction more rapidly than for free polymer chains.

In order to compare our experimental data with the behavior expected for hard sphere suspensions, we have

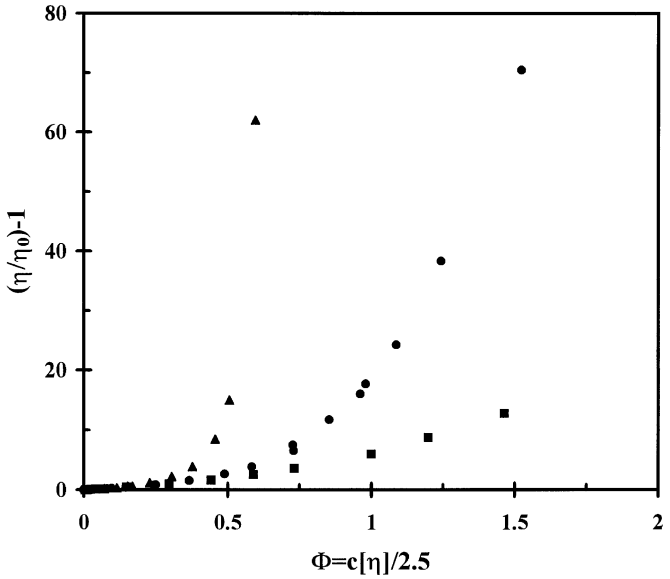

Fig. 3. Variation of $\eta/\eta_0 - 1$ *versus* volume fraction ($\Phi = c[\eta]/2.5$); (•) hairy particles, (▲) hard spheres (stearylated silica cores), (■) linear PDMS chains (same as the grafted one).

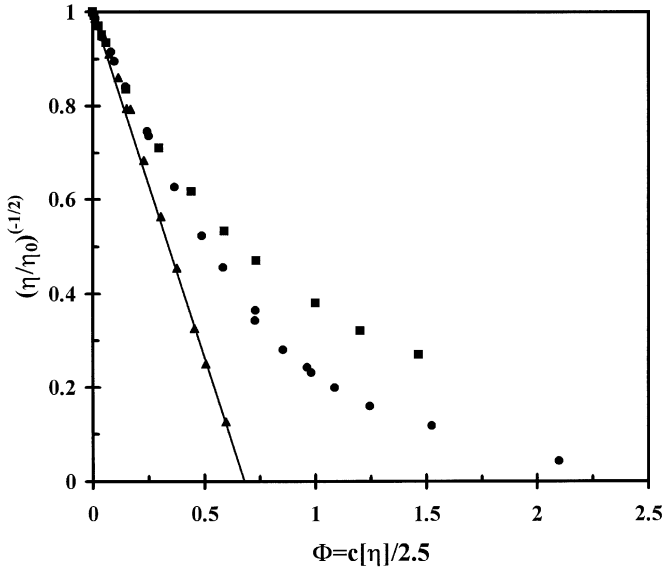

Fig. 4. Plot of $(\eta/\eta_0)^{-1/2}$ against volume fraction; (•) hairy particles, (▲) hard spheres, (■) linear PDMS chains.

reported in Figure 4 the variations of $(\eta/\eta_0)^{-1/2}$ *versus* Φ. Indeed, for hard sphere suspensions, recent theoretical and experimental studies have shown that the viscosity varies as [1,23,24]:

$$\eta = \eta_0 \left(1 - \frac{\Phi}{\Phi_{\rm cp}}\right)^{-2} \qquad (3)$$

where $\Phi_{\rm cp}$ is the maximum packing volume fraction: $\Phi_{\rm cp} \cong 0.63$ for hard spheres. A good agreement is observed for the suspension of stearic alcohol coated silica particles. With the representation used in Figure 4, all the points fall on a straight line as expected. The divergence of the

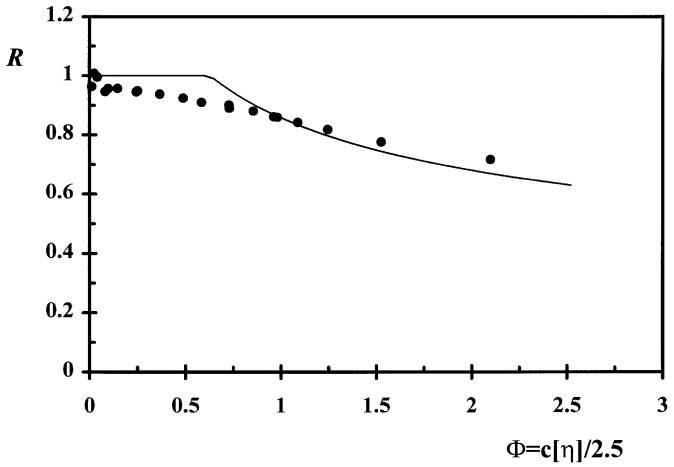

Fig. 5. Variation of the hairy grain effective radius with the particle volume fraction in dimensionless variables ($R = R_{\rm eff}/R_0$ *versus* $\Phi = c[\eta]/2.5$). The curve corresponds to idealized soft particles undergoing an affine collapse when Φ is larger than $\Phi_{\rm cp}$.

viscosity takes place for a volume fraction $\Phi_{\rm m} = 0.68 \pm 0.07$ which, within the error bar (mainly due to the uncertainty on $[\eta]$), is equal to the random close packing volume fraction $\Phi_{\rm cp}$.

Contrarily to hard spheres, hairy particles can compress or interpenetrate at high concentration. This property can be quantified by calculating an effective radius, $R_{\rm eff}$, of the particles: this radius corresponds to the radius of hard spheres giving the same viscosity for the same number of objects. The variation of $R = R_{\rm eff}/R_0$ with Φ is plotted in Figure 5 (R_0 is the value of $R_{\rm eff}$ for $\Phi \to 0$). We also report the variation calculated for idealized soft spheres that have a constant radius until close packing and that undergo an affine collapse for Φ larger than $\Phi_{\rm cp}$ (see Fig. 5).

From these results, we can also calculate the effective corona thickness: in dimensionless variable, $L = (R_{\rm eff} - a)/(R_0 - a)$. Figure 6 displays the variation of L *versus* the mean distance between the corona surface $h = 2(\Phi^{-1/3} - 1)R_0/(R_0 - a)$. For large h *i.e.* for very dilute suspensions, L equals 1. When h decreases *i.e.* for increasing values of Φ, the effective corona thickness decreases in agreement with what expected.

It is worth noting that R and L begin to vary well before the overlapping concentration. This result is related to the hairy particle structure. Indeed, even if in the very dilute regime, their behavior is the same as that of hard spheres (see Sect. 2), the corona permeability plays an important role for intermediate volume fractions where hydrodynamic interactions between the particles are dominant. As the particle volume fraction increases, R regularly decreases and L regularly increases but no singularity is observed around $\Phi \cong 1$. Recent experiments done on adsorbed polymer brushes also shown a continuous decrease of the hydrodynamic thickness before the polymer coated surfaces come into contact, and no anomaly of the hydrodynamic thickness variation at the brush

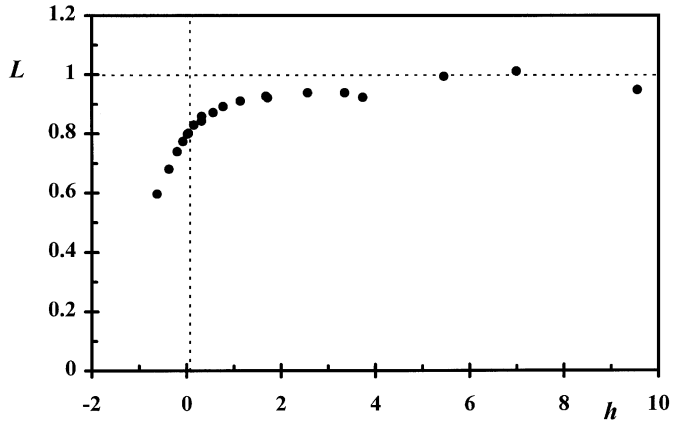

Fig. 6. Variation of the effective corona thickness with the mean distance between corona surface in dimensionless variables ($L = (R_{\rm eff} - a)/(R_0 - a)$ *versus* $h = 2(\Phi^{-1/3} - 1)R_0/(R_0 - a)$).

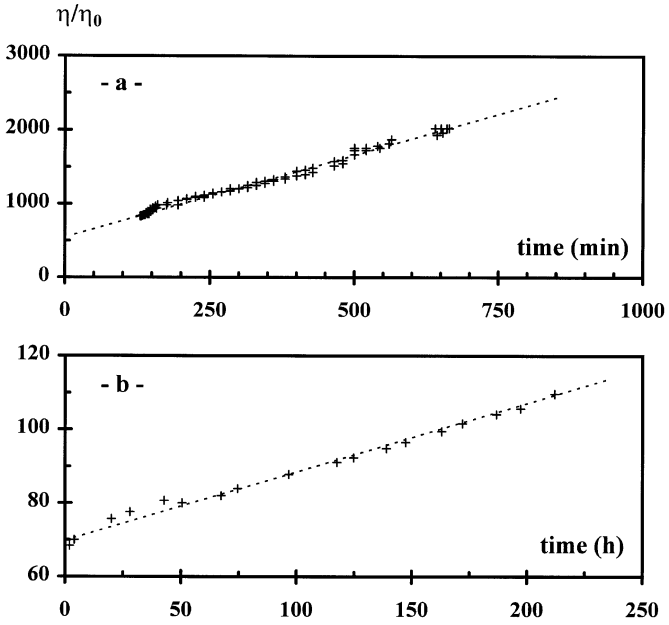

Fig. 7. Viscosity increase with time measured at short time: (a) $\Phi = 2.1$ ($c = 0.17$ g/cm^3); (b) $\Phi = 1.5$ ($c = 0.12$ g/cm^3).

overlap [25]. Various theories have modeled the flow of solvent inside grafted polymer layers using an analogy with a flow through a porous medium [25–28]. Even if the surfaces are far apart, the presence of a polymer layer leads to a decrease of the hydrodynamic interaction between the two surfaces. In the case of our particles, the very small curvature radius of the grafted polymer corona may also influence the flow penetration, and so the hydrodynamic interactions and the suspension viscosity.

Finally, it is interesting to compare the observed behavior with that found for different star-like polymer colloids. It has been shown that it mainly depends on the functionality of the stars [7]. For small arm numbers, behaviors similar to that we observed for the hairy particles have been found. On the contrary, for very large arm numbers, the star polymers are dense objects that do not interpenetrate: they exhibit exactly the same viscosity *versus* volume fraction dependence as hard spheres. In his work, Roovers gives a value of 64 arms as the limit separating the stars that easily deform and eventually interpenetrate from the stars that behave as hard spheres. The hairy particles we have synthesized have 55 arms; their behavior is not that of hard spheres corroborating the criterion introduced by Roovers [7].

5 Concentrated regime

In dilute state, the samples can be stored during long periods (several months) without any change in their viscosity. For large concentrations ($\Phi \geq 1.2$ *i.e.* $c[\eta] \geq 3$), on the contrary, their viscosity regularly increases and, after a certain time, the samples form a gel characterized by an elastic modulus. The kinetics of this time evolution strongly depends on the concentration: it is infinitely slow in dilute state and almost instantaneous for large concentrations ($\Phi \gg 2$ *i.e.* $c[\eta] \gg 5$). In an excess of solvent, the gels do not dissolve; a slight swelling takes place but, even after several months, the hairy particles do not redisperse. This shows that the bonds between the particles at the origin of gelation are irreversible. As mentioned in Section 1, it requires a special procedure to prepare the samples: the hairy particles can never be dried, and to avoid inhomogeneities, it is necessary that the concentration never locally reaches a large value. In practice, we studied the rheology of gelation using a suspension whose concentration was chosen equal to $c = 0.17$ g/cm^3 *i.e.* $\Phi = 2.1$.

Let us first consider the increase of the viscosity just after the sample preparation. At short time, the viscosity increases linearly (see Fig. 7). This allows us to easily find η at $t = 0$ (called $\eta_{\rm i}$) which corresponds to the values discussed in Section 3 and reported in Figure 3. From the observed variation, we can introduce a characteristic time: $\tau_0 = \eta_{\rm i}/({\rm d}\eta/{\rm d}t)_{t=0}$. For $c = 0.12$ g/cm^3, τ_0 equals 1.3×10^6 s (*i.e.* more than 15 days) and for $c = 0.17$ g/cm^3, τ_0 equals 1.7×10^4 s (about 2 days). This large difference illustrates the strong dependence of the kinetics on the concentration. This is also true for the gel time, $t_{\rm g}$, which is equal respectively to about 3 months for $c = 0.12$ g/cm^3 and 15 days for $c = 0.17$ g/cm^3. It is to note that $t_{\rm g}$ and τ_0 are expected to simply be proportional [29].

The sol-gel transition is characterized by a rapid increase of the viscosity followed by the appearance of an elastic modulus. In practice, in the vicinity of the gel point, the steady values of viscosity and elasticity are difficult to measure. For the hairy particle suspensions, the viscoelastic relaxation times are especially large. So, we used the procedure described in Section 1 to accurately determine the sol-gel transition time: for $c = 0.17$ g/cm^3, $t_{\rm g} = 3\,800 \pm 200$ min.

The critical behaviors of the viscosity and of the elastic modulus near $t_{\rm g}$ can be described by the following

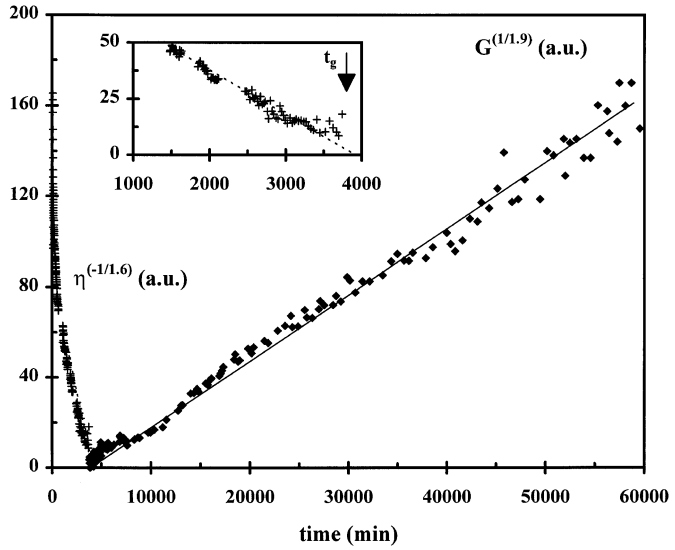

Fig. 8. Plot of $\eta^{-1/1.6}$ and $G^{1/1.9}$ against time for $\Phi = 2.1$ ($c = 0.17$ g/cm^3). Insert: detail of the curve near gelation point.

laws [30]:

$$\eta \propto \left(\frac{t_g - t}{t_g}\right)^{-\lambda} \quad \text{and} \quad G \propto \left(\frac{t - t_g}{t_g}\right)^{\kappa} \qquad (4)$$

where λ and κ are the exponents characterizing the critical behaviors of respectively the viscosity and the elastic modulus. In the frame of the scalar percolation theory, λ and κ are expected to be given by $0 \leq \lambda \leq 1.35$ and $\kappa = 1.9$ [30]. To fit our data with expressions (4), we plotted $\eta^{-1/x}$ and $G^{1/y}$ *versus* time (see Fig. 8). The value of λ (respectively κ) then corresponds to the value of x (respectively y) that leads to a linear variation in the vicinity of the gel point. This fitting procedure is more accurate than log-log plots which are very sensitive to the choice of t_g. We can also determine the extent of the critical domain *i.e.* the domain where expressions (4) hold.

In the sol domain ($t < t_g$), the exponent λ is found equal to 1.6 ± 0.3 and the critical domain extent: $(t_g - t)/t_g \cong 0.75$. The accuracy on λ is poor mainly because of the uncertainty on t_g. Near the gel point, the viscoelastic relaxation times are very long, and even if a very low gradient was used ($\cong 10^{-4}$ s^{-1}), the measured values may not be in the low shear rate limit. This explains the deviation of the last points with the best fitting curve (see insert in Fig. 8). In the gel domain ($t > t_g$), the critical behavior is observed to extend in a unusually large domain: $(t - t_g)/t_g \cong 23$. The exponent is then determined with a good accuracy: $\kappa = 1.9 \pm 0.1$. The values found for λ and κ are in very good agreement with the predictions of the scalar percolation model [30]. Large extents of the critical domain are expected for low concentration gels due to the importance of the connectivity fluctuations that then take place [31,32]. So, as a whole, the rheological results show a critical behavior of the sol-gel transition for the hairy particle suspensions very similar to that observed for usual polymer gels.

Gelation of a sterically stabilized colloidal suspension is rather unexpected, all the more so as the suspension is perfectly stable if it is dilute enough. Also puzzling is the fact that this process is irreversible. Experiments show that long grafted chains onto the silica surface are needed to induce sample gelation. Indeed, when the silica grains are stabilized by a dense coverage of short oligomers, no gelation takes place. Furthermore, for the same polymer as used here, but grafted onto particles having a 100 nm core radius, gelation occurs only at very high concentration, almost without solvent. On the contrary, gelation of hairy nanoparticle suspensions takes place in the presence of a large amount of solvent ($c \cong 0.1$ g/cm^3).

Several studies performed on star-shaped colloids (polymer stars or diblock copolymer micelles) have shown that solutions undergo an order-disorder transition at large concentration [7–9]. The existence of this transition depends on the functionality *i.e.* on the number of arms (see Sect. 3). It takes place near the close packing volume fraction $\Phi \cong 0.63$; the sample viscosity then increases sharply as for hard sphere suspensions. This differs from the gelation we observed. Furthermore, for all the star-shaped polymers investigated, the ordered state is reversible; it is destroyed under dilution. This is not the case of the hairy particle suspensions. The star-shaped polymer solutions can be prepared by adding solvent to dried samples, that is impossible in the case of hairy grains.

Various effects may be at the origin of the bonds formed at large concentration (these bonds are strong enough to impede the redispersion of the hairy particles-cohesion energy larger than kT). First, influence of the ungrafted polymer end has been checked. Indeed, although a reaction with silica at room temperature and without catalyst is highly improbable, the still active Si-OH end may play a role. In that aim, we used the monofunctional PDMS, synthetized by anionic polymerization: it carries at one end an unreactive sec butyl dimethyl silyl group and at the other end the same reactive SiOH group. Samples prepared with this polymer also gel. In both cases, after complete drying, the suspensions form transparent elastomers, highly resistant and stretchable. Second, we observed that the gelation of hairy particles strongly depends on the surface chemistry of the silica core. If the surface is completely saturated with short PDMS oligomers (the surface is treated with dimethylsiloxane trimers after the long chain grafting), the dried gel made by complete evaporation of the solvent loses its mechanical properties: it only has a low modulus and immediately tears under traction. This experiment supports the hypothesis that the bonds between the hairy particles are due to PDMS adsorption onto silica. This is not really a surprise: PDMS is known to strongly adsorb *via* H-bonds on various surfaces, among of them silica [33]. In the latter case, it has been shown more precisely that when adsorbed from solution, the chains are irreversibly bound to the surface and the amount of adsorbed polymer increases with the polymer volume fraction [34].

Let us now consider the influence of the concentration. In dilute regime, the polymer corona is fully stretched

with a decreasing monomer concentration profile (see Sect. 1). There is a repulsive interaction between two particles and it is not possible for a chain grafted onto a particle to penetrate the layer grafted onto another particle and reach its silica core. The suspension is then stable. Beyond the close packing volume fraction, the coronas start to overlap. According to the Daoud-Cotton model for star polymers [11], the space between two silica core is filled with blobs of equal size. The repulsive field around the particles is screened: there is a non-zero probability for "foreign" chains to come into contact with the silica core surface. Since the energy gain is low, the link should be reversible. But, the argument that explains the adsorption of high molecular weight polymer also holds here. The functionality of the hairy particles being large ($\cong$ 55 arms), there might be enough bonds to counterbalance the translational energy loss. However, the particle aggregation is very slow since it involves several particle collisions and the very slow dynamics of end-grafted polymers. In concentrated state, the average distance between particles is small, so a large interpenetration of the coronas is highly probable. In that case, the bonds form very rapidly: the gelation is almost instantaneous. It is interesting to note that the same (irreversible) gelation can also be induced by a very strong shearing of the suspension even at small volume fraction ($\Phi < 1$). The particle aggregation is due to the hydrodynamic forces that bring the particles into close contact and promote corona interpenetration [35].

Under complete drying, the suspensions form a transparent elastomer containing a high silica volume fraction (about 0.5). The cohesion of the material is totally insured by the bonding due to the grafted PDMS adsorption onto silica cores [2,12]. This elastomer can deform up to a large elongation ratio (8.6 ± 1.2) before breaking, the ultimate stress being 9 ± 1 MPa. These values are larger than those found for high performance reinforced silicon rubbers, showing that polymer/solid surface interaction is of major importance for the reinforcement of elastomers.

6 Conclusion

Suspensions of nanosized hairy particles exhibit original rheological behaviors. In dilute regime, the particles behave as stars with a very low flow penetration. The suspension is perfectly stable, and the hydrodynamic radius of the particles is very close to their external radius found in SANS experiments. However, hairy particles do not behave as hard spheres: the suspension viscosity does not diverge when the volume fraction reaches the close packing volume fraction. This is to be related to the number of arms ($\cong$ 55) which is large enough to avoid an important penetration of the flow at low volume fraction but not the interpenetration of the polymer corona at large volume fraction.

In concentrated regime ($\Phi \geq 1.2$), irreversible gels form; a sharp increase of the viscosity with time is followed by the appearance of an elastic modulus. Moreover, these gels swell but do not dissolve in an excess of solvent. We showed that the hairy particle bonding at the origin of this irreversible gelation is related to the core surface chemistry: one chain grafted onto a particle can absorb onto the silica core of another particle. So, this gelation does not occur if the polymer arms are too short or if the particle surface is treated to prevent adsorption. The critical behavior of the sol-gel transition is very similar to that of irreversible polymer gels; the exponents are in good agreement with scalar percolation predictions.

These original and unexpected properties are related to the architecture of the hairy particles. The thick grafted polymer layer is at the origin of a polymer star like behavior in dilute regime while the hard silica core dominates the properties at large concentration. Study of hairy particles with different architecture will be of great interest to understand the stability and rheology of sterically stabilized suspensions, these systems being well defined models for suspension investigations.

References

1. W.B. Russel, D.A. Saville, W.R. Schowalter, *Colloidal Dispersions* (University Press, Cambridge, 1989).
2. J.C. Castaing, C. Allain, P. Auroy, L. Auvray, A. Pouchelon, Europhys. Lett. **36**, 153 (1996).
3. B.J. Bauer, L.J. Fetters, W.W. Graessley, N. Hadjichristidis, G.F. Quack, Macromolecules **22**, 2337 (1989).
4. W.D. Dozier, J.S. Huang, L.J. Fetters, Macromolecules **24**, 2810 (1991).
5. J. Roovers, L.L. Zhou, P.M. Toporowski, M. van der Zwan, H. Iatrou, N. Hadjichristidis, Macromolecules **26**, 4324 (1993).
6. L. Willner, O. Jucknischke, D. Richter, J. Roovers, L.L Zhou, P.M Toporowski, L.J. Fetters, J.S. Huang, M.Y. Lin, N. Hadjichristidis, Macromolecules **27**, 3821 (1994).
7. J. Roovers, Macromolecules **27**, 5359 (1994).
8. G.A. McConnell, A.P. Gast, J.S. Huang, S.D. Smith, Phys. Rev. Lett. **71**, 2102 (1993).
9. D. Richter, O. Jucknischke, L. Willner, L.J. Fetters, M. Lin, J.S. Huang, J. Roovers, C. Toporovski, L.L. Zhou, J. Phys. France **3**, 3 (1993).
10. S. Forster, E. Wenz, P. Linder, Phys. Rev. Lett. **77**, 95 (1996).
11. M. Daoud, J.P. Cotton, J. Phys. France **43**, 531 (1982).
12. J.C. Castaing, *Stabilisation stérique de petites particules de silice monodisperses en solvant organique par greffage de longues chaînes de polydiméthylsiloxane et applications*, thèse de l'Université Paris VI, janvier 1996.
13. W. Stöber, A. Fink, E. Bohn, J. Colloid Interface Sci. **26**, 62 (1968).
14. G.H. Bogush, C.F. Zukoski, J. Colloid Interface Sci. **142**, 1 (1991).
15. see for instance *Handbook of Chemistry and Physics*, edited by R.C. Weast, (CRC Press, Boca Raton, Florida, 1983).
16. A.K. Van Helden, J.W. Jansen, A. Vrij, J. Colloid Interface Sci. **81**, 354 (1981).
17. J.C. Van der Werff, C.G. de Kruif, J. Rheol. **33**, 421 (1989).
18. C.G. de Kruif, E.M.F. van Iersel, A. Vrij, W.B. Russel, J. Chem. Phys. **83**, 4717 (1985).
19. D.A.R. Jones, B. Leary, D.V. Boger, J. Colloid Interface Sci. **147**, 479 (1991).

20. M. Adam, M. Delsanti, P. Pieranski, R. Meyer, Rev. Appl. Phys. **19**, 253 (1984).
21. B. Gauthier-Manuel, R. Meyer, P. Pieranski, J. Phys. E: Sci. Inst. **17**, 1177 (1984).
22. See for instance, S. T. Milner, Science **251**, 905 (1991); P. Auroy, L. Auvray, Langmuir **10**, 225 (1994)
23. D. Quemada, Prog. Colloid Polym. Sci. **79**, 112 (1989).
24. J.F. Brady, J. Chem. Phys. **99**, 567, (1993).
25. A. Dhinojwala, S. Granick, Macromolecules **30**, 1079 (1997).
26. G.H. Fredrickson, P. Pincus, Langmuir **7**, 786 (1991).
27. S.T. Milner, Macromolecules **24**, 3704 (1991).
28. A.A. Potanin, W.B. Russel, Phys. Rev. E **52**, 730 (1995).
29. C. Allain, L. Limat, L. Salomé, Phys. Rev. A **43**, 5412 (1991).
30. see for instance: C.J. Brinker, G.W. Scherer, *Sol-gel Science* (Academic Press Inc. San Diego, 1990).
31. M. Daoud, J. Phys. Lett. France **40**, 201 (1979).
32. C. Allain, L. Salomé, Macromolecules **23**, 981 (1990).
33. R. Iler, *The Chemistry of Silica* (John Wiley, 1979).
34. J-P. Cohen-Addad, C. Roby, M. Sauviat, Polymer **26**, 1231 (1985). L. Auvray, M. Cruz, P. Auroy, J. Phys. II France **2** (1992) 1133.
35. The gels induced by shearing are not homogeneous: we observed pieces of gel in the test tube. But one must be cautious about the interpretation of this last observation: indeed, we did not apply a controled shearing. We just shook the tube or in some cases, put it in an ultrasonic bath. Therefore, the inhomogeneity of the gel might reflect the inhomogeneity of the shearing.